Cellular/Molecular

The Fate of Synaptic Input to NG2 Glial Cells: Neurons Specifically Downregulate Transmitter Release onto Differentiating Oligodendroglial Cells

Maria Kukley,[1] Akiko Nishiyama,[2] and Dirk Dietrich[1]

[1]Department of Neurosurgery, University Clinic Bonn, D-53105 Bonn, Germany, and [2]Department of Physiology and Neurobiology, University of Connecticut, Storrs, Connecticut 06269

NG2-expressing oligodendrocyte precursor cells (OPCs) are ubiquitous and generate oligodendrocytes throughout the young and adult brain. Previous work has shown that virtually every NG2 cell receives synaptic input from many axons, but the meaning of this signaling is not understood. In particular, it is unclear whether neurons specifically synapse onto OPCs or whether OPCs merely trace adjacent neurotransmitter release sites and are not recognized by the presynaptic neuron. Here, we show with whole-cell recordings from distinct developmental stages of oligodendroglial cells in brain slices that synaptic input essentially disappears as soon as OPCs differentiate into premyelinating oligodendrocytes (NG2$^-$, DM20/PLP$^+$, O1$^+$). Uncaging experiments and tracer loading revealed that premyelinating oligodendrocytes still express a substantial number of AMPA/kainate receptors and many processes, but spontaneous and stimulated synaptic currents are mostly absent. Nevertheless, in a minority of premyelinating cells, electrical stimulation evoked small synaptic currents with an unusual behavior: their amplitude compared well with the quantal amplitude in OPCs but they occurred asynchronously and with the remarkable latency of 40–100 ms, indicating that the presynaptic release machinery has become ineffective. Mature myelinating oligodendrocytes completely lack AMPA/kainate receptors and respond to uncaging and synaptic stimulation with glutamate transporter currents. Our data show that neurons selectively synapse onto only one of several coexisting developmental stages of glial cells and thereby indicate that neurons indeed specifically signal to OPCs and are able to modulate transmitter output by regulating the local release machinery in a manner specific to the developmental stage of the postsynaptic glial cell.

Introduction

Cells expressing the NG2 proteoglycan (NG2 cells) are immature glial cells from which the vast majority of, if not all, oligodendrocytes are derived (Zhu et al., 2008a). It has now become clear that there is a dedicated signaling between neurons and NG2 cells. Although most types of glial cells respond in some way to extracellular neurotransmitter molecules, only NG2 cells receive classical synaptic input from neurons (Gallo et al., 2008). Neurons build up and maintain a fully competent release machinery at contact sites with NG2 cells and rapidly empty transmitter-filled vesicles in an action potential- and calcium-dependent manner. Released neurotransmitter, in turn, causes quantal synaptic currents in NG2 cells by the activation of neurotransmitter receptors (Bergles et al., 2000; Kukley et al., 2007).

Received Feb. 16, 2010; revised March 23, 2010; accepted April 3, 2010.

This work was supported by Deutsche Forschungsgemeinschaft Grants SFB TR3, DI 853/2, DI 853/3, and DI 853/4, and University Clinic Bonn grants (BONFOR). We are grateful to Boris Zalc, Jacky Trotter, and Bill Stallcup for generously providing antibodies, and to Elizabeth Matthews, Michel Royeck, and Reshmi Tognatta for critically commenting on this manuscript. We thank P. Stausberg, S. Buchholz, and J. Enders for their excellent technical assistance.

Correspondence should be addressed to Dr. Dirk Dietrich, Department of Neurosurgery, NCH U1 R035, Experimental Neurophysiology, University Clinic Bonn, Sigmund-Freud Strasse 25, D-53105 Bonn, Germany. E-mail: dirk.dietrich@ukb.uni-bonn.de.

M. Kukley's present address: Werner Reichardt Centre for Integrative Neuroscience, University of Tübingen, Paul-Ehrlich-Strasse 15-17, D-72076 Tübingen, Germany.

DOI:10.1523/JNEUROSCI.0854-10.2010

 0270-6474/10/308320-12$15.00/0

Synaptic signaling to NG2 cells occurs as early as these cells are generated, and this signaling is maintained while these precursor cells are proliferating and relocating in the brain (Kukley et al., 2008; Ge et al., 2009). This suggests that synaptic input may play a role in the early development of NG2 cells, and indeed there is evidence that the rate of division and the speed of migration can be modulated by the activation of neurotransmitter receptors on NG2 cells (Yuan et al., 1998; Tong et al., 2009).

It is tempting to speculate that other processes that occur in the later development of oligodendroglial cells could effectively be modulated by synaptic signaling as well. For example, because of its high temporal and spatial resolution, synaptic signaling from axons to NG2 cells would be ideally suited to instruct a differentiating oligodendroglial cell that myelination is required for a given individual axon in an activity-dependent manner (Gallo et al., 2008). However, for this scenario, synaptic input must either persist in later oligodendroglial developmental stages or have a significant long-term impact on NG2-positive precursor cells. Therefore, to elucidate possible roles and the involved mechanisms of the dedicated synaptic signaling from neurons to oligodendroglial cells, it is fundamental to precisely identify which developmental stage actually receives synaptic input from neurons.

During the period of myelination, the different stages of immature and mature oligodendroglial cells transiently coexist in the same area (Trapp et al., 1997). Furthermore, previous work

has shown that synapses on NG2 glial cells are formed by axon collaterals such that the glial cells are coactivated with the postsynaptic neuron (Bergles et al., 2000; Mangin et al., 2008; Müller et al., 2009). Therefore, certain neurons may have to signal in parallel to early and/or more mature oligodendroglial cells as well as to postsynaptically connected neurons. Clearly, the action potential will invade all axonal branches regardless of whether they synapse onto developing glial cells or onto neurons. It is therefore essential to know whether neurons are capable of orchestrating their synaptic output by differentially regulating the release machinery in a target-specific manner.

In this study, we recorded from different identified developmental stages of oligodendroglial cells in brain slices from transgenic mice and demonstrate that neurons indeed recognize the developmental stages of synaptically connected glial cells and modify their release machinery accordingly.

Materials and Methods

Electrophysiology

Hippocampal slices (300 μm thick) were prepared from 8- to 150-d-old transgenic mice expressing green fluorescent protein (GFP) under control of the proteolipid protein (PLP) promoter (PLP-GFP mice) (Fuss et al., 2000) or 8- to 16-d-old C57 black mice (Charles River). The brain was dissected in a solution of the following composition (in mM): 87 NaCl, 2.5 KCl, 1.25 NaH_2PO_4, 7 $MgCl_2$, 0.5 $CaCl_2$, 25 $NaHCO_3$, 25 glucose, 75 sucrose; osmolality, 300 mOsm/kg, pH 7.4, gassed with a 95% O_2 and 5% CO_2 mixture. Horizontal hippocampal slices were cut with a vibrating blade microtome (Leica Microsystems), and slices were quickly transferred to an interface incubation chamber and allowed to recover at 34°C for 30 min in the same solution as used for the dissection. Slices were then stored in the interface chamber at room temperature in artificial CSF (ACSF) containing the following (in mM): 124 NaCl, 3 KCl, 1.25 NaH_2PO_4, 2 $MgCl_2$, 2 $CaCl_2$, 26 $NaHCO_3$, 10 glucose; osmolality, 300 mOsm/kg, pH 7.4, gassed with a 95% O_2 and 5% CO_2 mixture. After a minimum of 1 h after preparation, individual slices were transferred to a submerged recording chamber mounted on the stage of an upright Nikon microscope (Nikon E600FN) and superfused continuously (~2 ml/min) with gassed ACSF. Drugs were added to this superfusion solution.

Whole-cell voltage-clamp experiments were performed using patch pipettes pulled from borosilicate glass on a vertical puller (model PP-830; Narishige). Electrodes had a resistance of 4–5 MΩ when filled with internal solution containing the following (in mM): 125 potassium gluconate, 10 HEPES, 0.5 EGTA, 2 $MgCl_2$, 2 Na_2-ATP, 20 KCl, 3 NaCl; pH adjusted to 7.3 with KOH, osmolality adjusted to 280–290 mOsm/kg. In some experiments (see below) measuring electrically stimulated synaptic currents, we used the following cesium-based internal solution (in mM): 150 Cs-gluconate, 2 $MgCl_2$, 2 Na_2-ATP, 0.5 EGTA, 10 HEPES; pH 7.3, osmolality adjusted to 280–290 mOsm/kg. Cesium was chosen to allow for better voltage control by blocking potassium currents when testing the reversal potential of asynchronous synaptic currents (see Fig. 4*D*). In total, 10 of the 15 experiments testing synaptic innervation of premyelinating oligodendrocytes with electrical stimulation were performed with the cesium-based solution. The remaining five experiments were performed with the potassium-based solution. Of six premyelinating oligodendrocytes with responses (including the transitional cell), four were recorded with cesium and two with potassium. Of the nine premyelinating oligodendrocytes that did not show synaptic responses, six were recorded with cesium and three with potassium. Cells recorded with the cesium-containing internal solution were not used for analyzing electrical properties or for measuring the resting membrane potential (data shown in Fig. 6).

The fluorescent tracer Lucifer yellow (0.1%) was included in the pipette solution for most of the experiments. Voltages were corrected for the liquid junction potential by offsetting the amplifier to −10 mV immediately before seal formation. Cells were voltage clamped at −80 mV with an EPC 7 amplifier (HEKA). The access resistance was regularly checked during the course of the recording and determined from the current response to a −5 mV hyperpolarizing voltage command and typically ranged between 10 and 25 MΩ. A low-resistance glass pipette (~1 MΩ) was used for monopolar extracellular stimulation of hippocampal axons nearby the recorded cell (pulses width of 0.1 ms applied once every 15 s).

All recorded currents were low-pass filtered at 3 kHz (except for miniature synaptic currents, which were filtered at 1 kHz), digitized with a sampling frequency of 10–20 kHz (ITC-16; InstruTECH), and acquired using custom-written routines in Igor Pro (Wavemetrics).

Cell selection and identification

Oligodendrocyte precursor cells (OPCs) were located visually in the CA1 stratum radiatum of the hippocampus using infrared–differential interference contrast videomicroscopy as described previously (Kukley et al., 2007, 2008). To verify the identity of the selected cells and to establish a reliable and simple electrophysiological criterion to distinguish different types of glial cells in the postnatal hippocampus, we performed an additional and extensive series of postrecording immunohistochemical stainings for different glial and neuronal markers. These data are presented in the supplemental material (supplemental Figures 3–7, available at www.jneurosci.org). In addition, the routine inclusion of the tracer Lucifer yellow into the pipette solution allowed the morphological assessment of cell identity. Of the 21 OPCs presented in the main part of this manuscript (i.e., excluding the cells from the supplemental material, available at www.jneurosci.org), 9 were recorded in PLP-GFP transgenic mice and 12 were recorded in wild-type mice. When recording OPCs in transgenic mice, we avoided selecting fluorescent cells as they represent more mature oligodendroglial cells (for more details, see Results). We did not note any differences between OPCs recorded in wild-type mice and those recorded in PLP-GFP transgenic mice. The age of the mice in which we recorded OPCs ranged between postnatal day 9 (P9) and P14.

Premyelinating oligodendrocytes were identified with the help of PLP-GFP mice (Fuss et al., 2000) at the age of P9–P15. In this mouse line, mature oligodendrocytes appear as brightly fluorescent cells as described previously. In addition, we discovered a population of weakly fluorescent cells in live brain slices, the majority of which we identified as premyelinating oligodendrocytes (the remaining cells were young oligodendrocytes displaying a small number of sheaths) (for details, see Results). Using Lucifer yellow filling of the cells during patch-clamp recordings, we confirmed the absence of myelin sheaths and the typical cellular morphology for each cell included in the study as premyelinating oligodendrocyte (cf. Trapp et al., 1997). We further verified that NG2 cells did not express GFP in these mice (see supplemental Fig. 8, available at www.jneurosci.org as supplemental material). Premyelinating oligodendrocytes occurred much less frequently than OPCs and also less frequently than myelinating oligodendrocytes. Beyond that, premyelinating oligodendrocytes were most rarely encountered in those areas of the hippocampus that are least myelinated (see Fig. 1*A*). For this reason, some of the cells were collected in other hippocampal areas. In detail, of 38 premyelinating oligodendrocytes, 27 were recorded in CA1 stratum radiatum, 3 in CA1 stratum lacunosum moleculare, 4 in CA2/CA3 stratum radiatum, and 4 in subiculum. The cells were pooled as we could not detect any differences between them.

Myelinating oligodendrocytes were easily identified by selecting brightly fluorescent cells in the PLP-GFP transgenic mice. Tracer loading revealed the presence of myelin sheaths in these cells. Myelinating oligodendrocytes were recorded in mice of two age groups: the first group comprised oligodendrocytes recorded in mice aged between postnatal day 35 and 50, and the second group consisted of those recorded in 3- to 5-month-old animals. Of 39 oligodendrocytes, 31 were recorded in CA1 stratum radiatum, 1 in CA1 stratum lacunosum moleculare, 6 in CA2/CA3 stratum radiatum/lacunosum, and 1 in subiculum. Because we did not find differences in the physiology or the morphology between both groups of oligodendrocytes, the data were pooled.

Flash photolysis

We used an electrically triggered xenon flash lamp (Rapp OptoElectronic) to deliver a brief (τ = 0.6 ms) pulse of UV light (300–390 nm; filter UV-2) to the slice tissue. The light of the lamp was fed into a light

guide (400 μm diameter) whose other end was positioned directly above the brain slice. The tip of the light guide was positioned ~0.5 mm above the slice surface and positioned such that the recorded cell was in the center of the UV spot. The spot was visualized on the slice surface by an alternate coupling of a deep red laser into the light guide and was estimated to cover an area of ~600 × 900 μm. Throughout this study, we used only one of the three built-in capacitors (1000 μF) charged to 250 V to generate the light arc. According to the calibration of the manufacturer, these settings generate ~2 mJ per flash at the light guide terminal. In each cell, we verified that a flash of UV light alone, in the absence of caged neurotransmitter, does not produce any current changes or any photodamage. For bath application of caged glutamate, *N*-(α-carboxy-2-nitrobenzyl) ester, trifluoroacetic acid salt caged glutamate (Invitrogen), we stopped the perfusion and added 50 μl of a caged glutamate stock solution to the fluid volume in the chamber to yield a final concentration of 250 μM. After adding the caged glutamate, we waited 8 min before the experiment was started to allow for diffusional equilibration of the drug within the chamber. In each cell, only one flash response was registered to avoid confounding the results by varying depletion of caged glutamate by preceding flashes. For antagonist experiments, cells were equilibrated with the blocker before the first flash.

Analysis

Spontaneous miniature synaptic currents were analyzed by the sliding template algorithm provided by NeuroMatic (V1.71) for Igor Pro (V5) with a threshold of 3. The template chosen closely matched quantal synaptic currents and displayed a rise time and a decay time of 1 and 2 ms, respectively. All detected events were visually inspected and discarded in case of doubt. In each cell, an average was calculated across all events, and kinetic parameters as well as the amplitude were determined from this mean current. We analyzed a recording period of 9 ± 1 min ($n = 13$) for the occurrence of synaptic currents in each cell. To account for the fact that random noise occasionally can create spurious synaptic events, we used the following rule to define a "responder": we define our error threshold at four events per 5 min (i.e., a cell showing four or fewer events per minute we classified as "nonresponder"). This was the case for one premyelinating oligodendrocyte (four events in 12 min) and for two oligodendrocytes (two events in 5 min and four events in 12 min). For comparison, in OPCs, we recorded between 120 and 360 events per 5 min.

Calculation of passive-cell properties. Series resistance, R_S, was estimated from transient currents in response to a small voltage step ($\Delta V = -10$ mV). Membrane resistance, R_m, was calculated as difference between the total resistance, obtained from the steady-state current in response to a small voltage step, and the series resistance, R_S. Cell capacitance, C_m, was derived from the charge transferred into cell capacitance (ΔQ) by the following procedure. Let $\Delta I_{total}(t)$ denote the measured, time-dependent change in current during application of ΔV. The capacitive current $I_C(t)$ was then calculated as the difference between total and resistive current (onset of voltage step at $t = 0$) as follows:

$$I_C(t) = \Delta I_{total}(t) - \frac{\Delta V - \Delta I_{total}(t) * R_S}{R_m}.$$

The area under $I_C(t)$ approximates ΔQ and was transformed into cell capacitance, C_m, according to the following:

$$C_m = \frac{\Delta Q * (R_m + R_S)}{R_m * \Delta V},$$

resting membrane potential = zero current potential.

Voltage-activated currents. Peak amplitudes of sodium currents, transient and sustained potassium currents were quantified from current responses to voltage steps from holding potential ($V_h = -80$ mV) to +10 mV. All values were determined from leak-subtracted current traces.

Immunohistochemistry

Immunohistochemistry. Slices after an electrophysiological experiment or tissue blocks freshly prepared as described above were fixed overnight in 8% paraformaldehyde (in PBS) and then resectioned at 40–50 μm using a vibratome. Electrophysiologically investigated slices were embedded in agar to facilitate resectioning. Immunohistochemical stainings were then performed according to one of the following four protocols: (1) primary antibodies (ab) overnight in TBS plus 0.2% Triton X-100, secondary ab and detection, each applied for 4 h in TBS plus 0.2% Triton X-100; (2) primary ab 3 d in TBS, secondary ab and detection, each applied overnight; (3) 5 min microwave pretreatment in citrate buffer, primary ab overnight in TBS plus 0.2% Triton X-100, secondary ab and detection, each applied for 4 h in TBS plus 0.2% Triton X-100; (4) 5 min microwave pretreatment in citrate buffer, primary ab overnight in TBS, secondary ab and detection, each applied overnight. Secondary detection was usually performed by biotinylated secondary antibodies (1:200–1:50), followed by incubation with streptavidin-Cy5 or -Cy3 (1:200; Jackson ImmunoResearch). In some cases dye-conjugated secondary antibodies were used (e.g., anti-rabbit-RRX). For counterstaining of nuclei, we used dyes of the fluorescent Nissl stain series (1:100; Neurotrace; Invitrogen) in either Cy2, Cy3, or Cy5 emission range. The supplemental Materials and Methods (available at www.jneurosci.org as supplemental material) gives details on which primary antibodies were used.

Image acquisition and analysis. Sections were analyzed with a confocal laser-scanning microscope (Leica TCS NT, equipped with an argon–krypton laser), and images with different dyes (e.g., Lucifer yellow, Cy3 and Cy5) were acquired sequentially. For LY/equivalents, the following filters and laser lines were used: excitation, 488 nm; dichroic, 510 nm; emission bandpass, 530/30 nm. For Cy3/equivalents, we used the following: excitation, 568 nm; DD488/568; pass-through dichroic, 580 nm; emission bandpass, 600/30 nm. For Cy5/equivalents, we used the following: excitation, 647 nm; dichroic, 660 nm; emission long pass, 665 nm. The majority of scans were acquired with a 63× objective [oil, numerical aperture (NA) 1.4, or water with correction collar, NA 1.2], and the pinhole was set to 1 Airy unit. Laser power, detector gain, and offset were adjusted such that, in the final scan (4–10 averages), only a few pixels had zero or maximal (255) digital units. Typically, detector gain and offset were set to ~70% and ~6 digital units, respectively. To preserve visibility of details in small-sized images, figure postprocessing was necessary (Photoshop): maximum brightness was rescaled to 80–100%, and a gamma correction factor of ~1–1.3 was introduced.

Results

For this study, we have chosen the CA1 area of the hippocampus as a partially myelinated (Fig. 1*A*) and synapse-rich model system. It is known that all NG2 cells in the postnatal CA1 region are contacted by synapses from surrounding axons (Bergles et al., 2000; Kukley et al., 2008). Therefore, this region enables us to investigate the developmental fate of synaptic connections to NG2 cells when they differentiate into oligodendrocytes while at the same time synaptic connections to neighboring neurons are maintained. As can be seen in Figure 1*A*, despite the fact that the hippocampus is a gray matter structure, there is a significant amount of myelin in certain dendritic subfields in the adult mouse, which requires the generation of oligodendrocytes.

To verify in our system that these oligodendrocytes are generated from NG2 cells and to define the transitional stages during the process of differentiation, we used a transgenic approach described previously (Zhu et al., 2008a). We crossed mice expressing Cre recombinase in NG2 cells (NG2Cre mice) with Z/EG Cre reporter mice (Novak et al., 2000) to be able to identify the progeny of NG2 cells based on cellular expression of GFP. This NG2cre:Z/EG double-transgenic mouse line has previously been used to study the fate of NG2 cells in other brain regions (Zhu et al., 2008a,b). With the help of these mice, we identified three different main stages of oligodendroglial cells in the CA1 region (Fig. 1*B–O*). Until around P8, all GFP-positive cells were also positive for NG2, identifying them as OPCs. These cells constitute the class of OPCs characterized by a small polygonal soma and a multipolar tree of delicate processes (Fig. 1*B*,*C*).

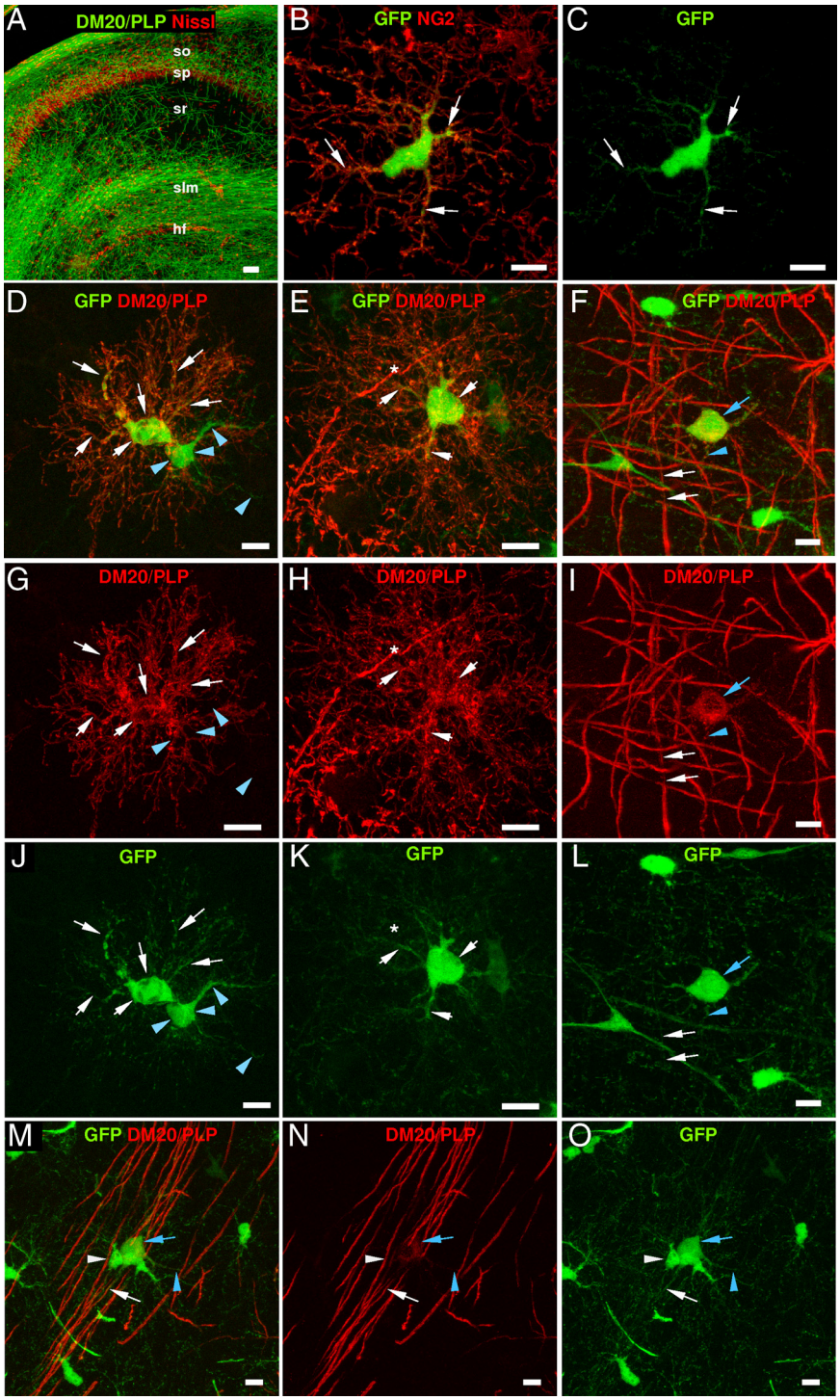

Figure 1. Hippocampal NG2 cells generate myelinating oligodendrocytes. ***A***, Single plane of a dual-channel confocal scan of the hippocampal CA1 region of a 3-month-old mouse showing the myelin distribution. Myelin is stained with antibodies against DM20/PLP (green), and nuclei are in red. Note that some fiber tracts such as the slm are heavily myelinated despite the fact that the hippocampus represents a gray matter structure. Scale bar, 50 μm. so, Stratum oriens; sp, stratum pyramidale; sr, stratum radiatum; slm, stratum lacunosum moleculare; hf, hippocampal fissure. ***B***, Double labeling for NG2 and GFP in a NG2cre:Z/EG double-transgenic mouse at P6. An NG2- and GFP-positive cell in the stratum radiatum of the CA1 region is shown. The arrows point to NG2-positive processes that also contain GFP immunoreaction product. Scale bar, 10 μm. This image and all images displayed in ***C–O*** represent a maximum projection along ~5 μm of the *z*-axis of a stack of confocal scans centered at the soma. ***C***, GFP channel of the image shown in ***B***. ***D***, GFP-positive premyelinating oligodendrocyte in the stratum radiatum of a NG2cre:Z/EG mouse (P10) identified by its typical morphology. Notice the DM20/PLP staining all over the surface of the cell and the absence of any myelin sheaths. Also note that the immunostaining of premyelinating oligodendrocytes by antibodies against DM20/PLP is much weaker than the staining of myelin sheaths such as shown in ***A***. This difference can best be appreciated in images that display both a premyelinating oligodendrocyte and myelin. Because the gain of the scan system has to be increased to adequately sample the premyelinating oligodendrocyte myelin structures appear strongly saturated (***E***, ***H***) [Kukley et al. (2007), their Fig. 6*F*]. The white arrows point to processes and the soma of the GFP-positive premyelinating oligodendrocyte. The blue arrowheads point to a GFP-positive cell that did not label with DM20/PLP antibodies and that presumably represents an OPC. Scale bar, 10 μm. ***E***, GFP-positive young oligodendrocyte in the stratum radiatum of a NG2cre:Z/EG mouse (P10). This cell looks very similar to the one shown in ***C***, but it additionally shows at least one myelin sheath (as indicated by the asterisk). The white arrows denote the GFP-positive soma and processes of this cell. Scale bar, 10 μm. ***F***, Mature myelinating oligodendrocyte in the stratum radiatum of a NG2cre:Z/EG mouse (P18). At this developmental stage, the soma (blue arrow) and the thin processes (blue arrowhead) connecting the cell body to myelin sheaths (white arrows) are only weakly labeled by DM20/PLP antibodies. Note the random orientation of the myelin sheaths, which reflects the orientation of axons in stratum radiatum. Scale bar, 10 μm. ***G–L***, Single-channel scans corresponding to ***D–F***. Labels are placed at exactly the same position for comparison. ***M***, Mature oligodendrocyte in the same animal as shown in ***E*** but located in stratum lacunosum moleculare. Note the parallel course of the myelin sheaths in this layer, which more closely resemble the appearance of white matter oligodendrocytes. The symbols are as in ***E***. To the left of the cell body of this oligodendrocyte, there is a small DM20/PLP-negative cell that presumably represents an OPC (white arrowhead). Scale bar, 10 μm. ***N***, ***O***, Single-channel scans corresponding to ***I***.

Thereafter, a second class of GFP-positive cells occurred, which were significantly larger and showed a more complex tree of heavily branching processes (Fig. 1*D*,*G*,*J*). The processes were longer when compared with NG2 cells and spanned an approximately circular area. Typically, some bulky processes emanated from the soma, which branch most heavily in distal areas. These cells are distinct from OPCs as they are labeled by antibodies specific for PLP and its DM20 splice variant and as they typically do not show immunoreactivity to NG2 antibodies anymore (supplemental Fig. 1, available at www.jneurosci.org as supplemental material) (Trapp et al., 1997; Mallon et al., 2002; Nishiyama et al., 2009). Importantly, these cells did not show any myelin sheaths and their entire surface was labeled with PLP/DM20 antibodies (Fig. 1*G*). Together, the appearance of these cells was typical of premyelinating oligodendrocytes that have been described in gray and white matter regions throughout the CNS during the period of myelination (Trapp et al., 1997; Mallon et al., 2002).

Starting at P13, the earliest members of the third class, the myelinating oligodendrocyte, were observed. These GFP-positive cells are very similar to the just-described premyelinating oligodendrocytes but now show one to two myelin sheaths that were heavily labeled by the PLP/DM20 antibodies (Fig. 1*E*,*H*,*K*).

Finally, at around P18, the first GFP-positive cells representing fully mature myelinating oligodendrocytes were found in the CA1 region. Note, that whereas the sheaths were very strongly labeled by the PLP/DM20 antibodies, the surface of the soma and of the processes connecting the soma to the sheaths was hardly visible in these mature cells (Fig. 1*F*,*I*,*L*,*M–O*). In fact, the labeling of processes and the soma was much weaker than that of premyelinating oligodendrocytes (Fig. 1*M–O*).

To test for the presence of functional synaptic connections to these different developmental stages of oligodendroglial cells, we obtained whole-cell patch-clamp recordings in acute brain slices prepared from wild-type and transgenic mice. During the recording, we filled cells with the tracer Lucifer yellow, which allows the identification of the recorded cells by characterizing their antigen profile through postrecording immunohistochemistry and by confirming their detailed cellular morphology (Fig. 2). We used dye-filled OPCs and premyelinating oligodendrocytes ($n = 4$ for each type) for a detailed morphometric analysis (supplemental Fig. 2, available at www.jneurosci.org as supplemental material). As expected from the GFP expression pattern shown in Figure 1, premyelinating oligodendrocytes display a significantly larger total process length (2891 ± 177 vs 1198 ± 190 μm), area covered by the processes (6169 ± 235 vs 3328 ± 215 μm^2), and diameter of the soma (9.7 ± 0.9 vs 6.5 ± 0.7 μm) when compared with OPCs.

First, we aimed at quantifying glutamatergic synaptic input to NG2 cells in hippocampal slices prepared from mice at P9–P14. In our previous work, we identified NG2 cells based on their small size and their characteristic current pattern dominated by voltage-gated outward currents (Kukley et al., 2008).

Recently, it was reported that NG2 cells in cerebellar white matter are heterogeneous with respect to the expression of voltage-gated sodium channels (Káradóttir et al., 2008) (but see Gallo et al., 2008). Because we have not seen this heterogeneity in our previous work (Kukley et al., 2007, 2008), we wondered whether our criteria may somehow only select a subpopulation of NG2 cells. To verify that our selection criterion is specific for OPCs and includes the vast majority of the population of NG2 cells, we correlated the current pattern of many glial cells ($n = 108$, total number of cells analyzed by postrecording immunohistochemistry). The full results are shown in supplemental Figures 3–7 (available at www.jneurosci.org as supplemental material) and clearly suggest in the region and age analyzed that (1) our selection criteria specifically identify NG2 cells, and selected cells well represent the entire population of NG2 cells; (2) all NG2 cells show fast sodium currents; (3) NG2 cells do not express markers of more mature oligodendroglial cells like DM20/PLP, O1, or CD9; and (4) different types of glial cells can safely be distinguished based on their current pattern.

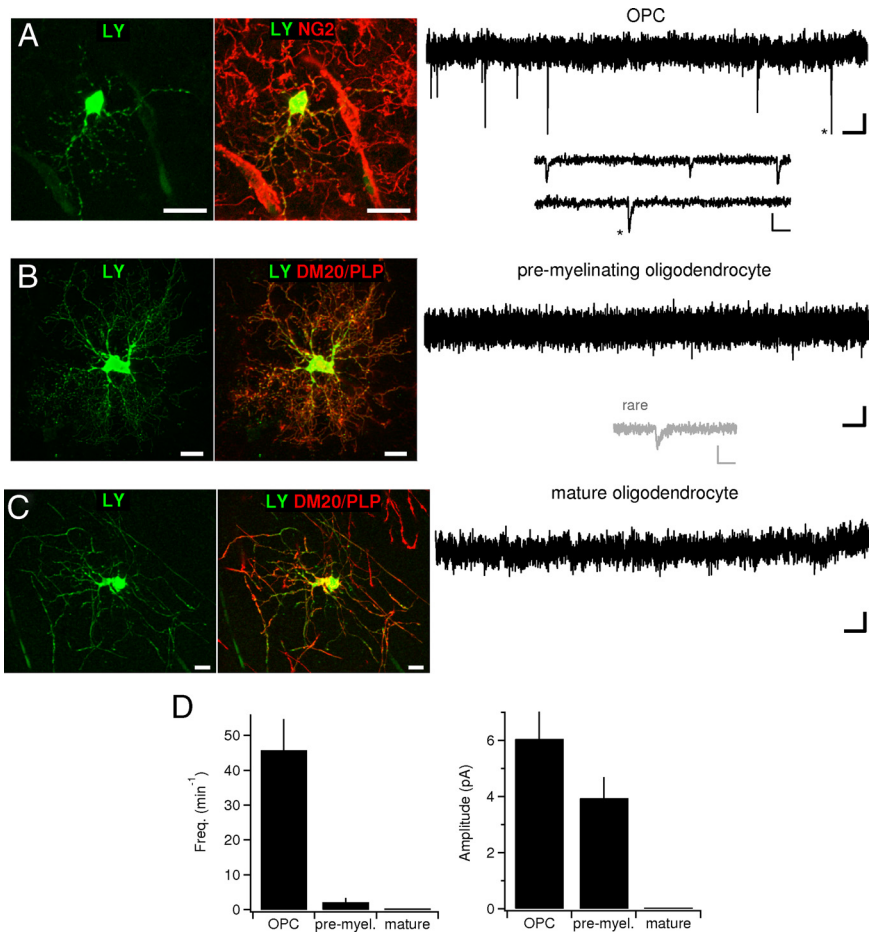

Figure 2. Synaptic input is rapidly lost on differentiation. ***A***, Left and middle, Single- and dual-channel confocal scan of a NG2-positive cell in CA1 stratum radiatum that was filled with Lucifer yellow during the whole-cell recording. The electrophysiology of this cell is shown on the right. Scale bar, 10 μm. Right, Continuous whole-cell voltage-clamp recording of ruthenium red-evoked miniature EPSCs obtained in the NG2-positive OPC shown on the left. Calibration: 0.2 s, 2 pA. Inset, Part of the top trace is shown at an expanded timescale to illustrate the fast kinetics of the spontaneously occurring inward currents. The asterisks denote corresponding events in both traces. Calibration: 20 ms, 5 pA. ***B***, Left and middle, Single- and dual-channel confocal scan of a DM20/PLP-positive cell in CA1 stratum radiatum filled with Lucifer yellow during the whole-cell recording. The electrophysiology of this cell is shown on the right. Scale bar, 10 μm. Right, Continuous voltage-clamp recording of premyelinating oligodendrocyte shown on the left. Note the lack of spontaneous inward currents despite the presence of the secretagogue ruthenium red. Calibration: 0.2 s, 2 pA. Inset (gray), Very rarely, we observed spontaneous currents closely resembling synaptic currents frequently occurring in OPCs. See text for details. Calibration: 20 ms, 5 pA. ***C***, Left and middle, Single- and dual-channel confocal scan of a mature myelinating oligodendrocyte in CA1 stratum radiatum filled with Lucifer yellow and displaying numerous PLP-positive myelin sheaths. Scale bar, 10 μm. Right, Continuous whole-cell recordings of the oligodendrocyte shown on the left. We never encountered synaptic currents in this type of cell. Calibration: 0.2 s, 2 pA. ***D***, Left, Summary bar graph depicting the mean frequencies of miniature synaptic currents in the three developmental stages of oligodendroglial cells investigated. OPCs, 46 ± 9 per minute ($n = 4$); premyelinating oligodendrocytes, 2.2 ± 1.2 per minute ($n = 5$); mature oligodendrocytes, 0 per minute ($n = 4$). Right, Summary of the mean amplitudes of miniature synaptic currents. Only cells in which synaptic events were detected are included in these numbers. OPCs, 6 ± 0.9 pA ($n = 4$); premyelinating oligodendrocytes, 4 ± 0.7 pA ($n = 4$); no events were detected in mature myelinating oligodendrocytes. Note that the estimates of the amplitude of miniature currents in the group of premyelinating oligodendrocytes is not very robust as only few events were detected (in total, 82 events in 4 cells) and probably reflects a lower limit because we tended to count even very small deflections in order not to falsely miss any small remaining synaptic input. Error bars indicate SEM.

To test for synaptic input to these NG2 cells, we blocked $GABA_A$ receptors (10 μM bicuculline) and action potentials (1 μM TTX) and provoked vesicular release by bath-applying 100 μM ruthenium red. Before application of this drug, the frequency

of spontaneous synaptic currents was very low and amounted to 3.8 ± 1.5 events per minute (data not shown) ($n = 4$). As reported previously (Lin and Bergles, 2004; Kukley et al., 2007, 2008; Kukley and Dietrich, 2009), application of ruthenium red consistently induced small, spontaneous, and frequent inward currents in every OPC tested (frequency, 46 ± 9 events per minute; $n = 4$) (Fig. 2*A*). These currents showed the characteristic fast kinetics typical of AMPA/kainate-mediated miniature synaptic currents in OPCs (amplitude, 6.1 ± 0.97 pA; rise time, 0.4 ± 0.02 ms; decay time constant, 1.9 ± 0.2 ms) (Bergles et al., 2000; Kukley et al., 2007, 2008; Ziskin et al., 2007).

We next asked whether spontaneous synaptic currents can still be detected in cells that have evolved into premyelinating oligodendrocytes. Because premyelinating oligodendrocytes are a transient developmental stage that exists only for ~2–3 d (Trapp et al., 1997), their occurrence is rare compared with OPCs especially in weakly myelinated areas. To facilitate the identification of those cells, we used a transgenic mouse line that expresses GFP under the PLP promoter (Fuss et al., 2000). In this mouse line, expression of GFP is restricted to more mature, NG2-negative cells of the oligodendroglial lineage (supplemental Fig. 8, available at www.jneurosci.org as supplemental material), whereas in the above-mentioned NG2cre:Z/EG mice all stages of oligodendroglial cells express GFP. To select premyelinating versus mature oligodendrocytes, we chose cells for patch-clamp recordings displaying a very weak GFP fluorescence. Additionally, we verified that the recorded and dye-filled cell did not display any sheaths. Cells selected in this manner were stained by the PLP/DM20 antibodies ($n = 6$) (Fig. 2*B*) and by O1 antibodies ($n = 4$) (data not shown) in all tested cases and showed the typical labeling of the entire surface confirming their identity as premyelinating oligodendrocytes (Sommer and Schachner, 1981; Trapp et al., 1997).

We provoked vesicular release from nerve terminals in exactly the same way as used for NG2-positive OPCs (100 μM ruthenium red; before application we did not detect any spontaneous synaptic currents; $n = 5$). However, in striking contrast to the high frequency of spontaneous synaptic currents in OPCs, spontaneous synaptic currents were rarely observed in premyelinating oligodendrocytes (Fig. 2*B*). In one of five cells, no synaptic currents could be detected, and in the remaining four cells the frequency of occurrence dropped ~20-fold when compared with OPCs (frequency, 2.2 ± 1.2 per minute; $n = 5$; $p < 0.0201$) (Fig. 2*B*,*D*). The amplitude and the kinetics of the few spontaneous currents registered in premyelinating oligodendrocytes were comparable with the currents recorded in OPCs (Fig. 2*B*, inset; *D*) (amplitude, 4.0 ± 0.74 pA; rise time, 0.5 ± 0.07 ms; decay time constant, 2.4 ± 0.19 ms; $n = 4$; not significantly different from the values of OPCs).

To test for synaptic input to myelinating oligodendrocytes, we selected brightly fluorescent cells in the PLP-GFP transgenic mouse line. These cells clearly displayed myelin sheaths, varying between only a few up to many (Fig. 2). In all of the myelinating oligodendrocytes, no spontaneous synaptic currents could be detected (Fig. 2*C*,*D*) ($n = 4$). Together, the data so far show that the occurrence of spontaneous synaptic currents is highly restricted to the oligodendroglial cells in the stage of NG2-expressing OPCs.

We next asked whether the lack of synaptic responses in premyelinating and myelinating oligodendrocytes is attributable to a reduced responsiveness to glutamate caused by a developmental downregulation of functional glutamate receptors. To address this question directly, we exposed the entire surface of the cells to fast photolytic release of glutamate (uncaging). We patch clamped OPCs, premyelinating and myelinating oligodendrocytes and bath applied 250 μM caged glutamate (biologically inactive) in the presence of NMDA and $GABA_A$ receptor antagonists (50 μM APV; 10 μM bicuculline) and TTX (0.5 μM). We then uncaged glutamate by a brief flash of UV light (<1 ms) while the cell was held in voltage-clamp mode at −80 mV.

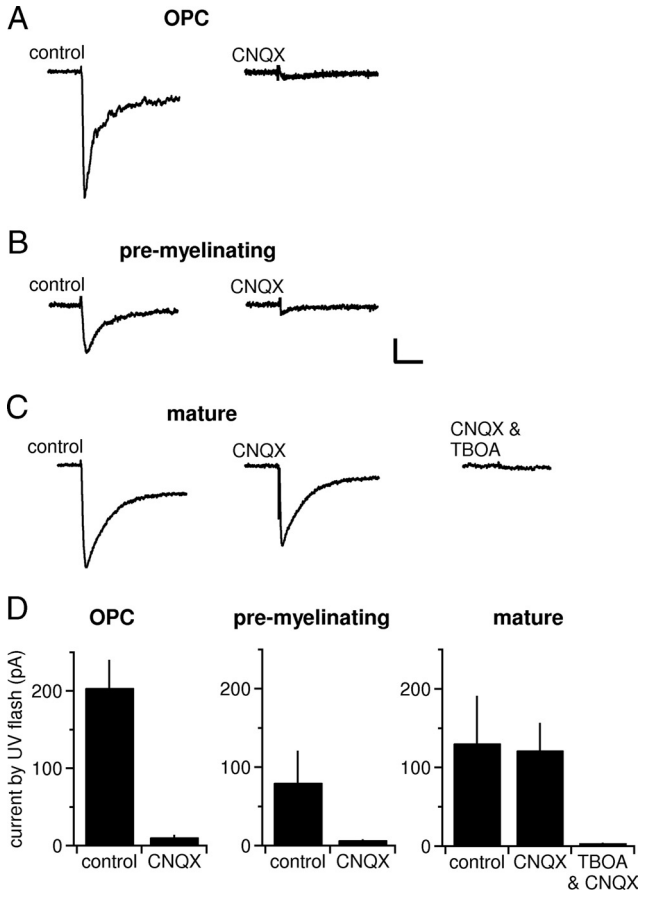

Figure 3. Glutamate responsiveness is maintained in premyelinating and mature oligodendrocytes. ***A***, Whole-cell current responses (−80 mV, holding potential) of OPCs to photolytic release of glutamate in the absence (left) and presence (right) of the AMPA/kainate receptor antagonist CNQX. The prominent fast inward current observed under control conditions is prevented by preapplication of CNQX. Calibration is as in ***B***. ***B***, Premyelinating oligodendrocytes also show a CNQX-sensitive response to photolytic release of glutamate (−80 mV). Calibration: 20 ms, 30 pA. ***C***, The response to glutamate by mature oligodendrocytes is resistant to CNQX but was blocked by the glutamate transporter antagonist TBOA (−80 mV). Calibration is as in ***B***. ***D***, Summary bar graphs of the current amplitudes recorded on glutamate uncaging in the three developmental stages measured in the absence and presence of blockers as shown in ***A–C***. The bar graphs represent absolute current amplitudes as given in the main text. The current densities (in picoamperes per picofarad) are as follows (from left to right): 7.6 ± 1.1, 0.3 ± 0.06, 1 ± 0.5, 0.1 ± 0.02, 1.8 ± 1.3, 0.5 ± 0.1, and 0.04 ± 0.01. Error bars indicate SEM.

As expected, uncaging glutamate onto OPCs produced a pronounced fast rising inward current of 204 ± 36 pA ($n = 4$), which was prevented by the AMPA/kainate receptor antagonist CNQX (11 ± 2.9 pA; $n = 2$; 30 μM) (Fig. 3*A*,*D*).

Similarly, in premyelinating oligodendrocytes, we also consistently observed a clear inward current on uncaging glutamate (80 ± 40 pA; $n = 5$) (Fig. 3*B*,*D*), which corresponds to approximately one-half of the current observed in OPCs. This current showed comparable kinetics and was also prevented by CNQX (7.3 ± 0.8 pA; $n = 4$; 30 μM) (Fig. 3*B*). Therefore, despite the dramatic reduction of their synaptic input, premyelinating oligo-

dendrocytes are still responsive to glutamate and express a substantial number of AMPA/kainate type of glutamate receptors.

Surprisingly, even mature oligodendrocytes responded with prominent and rapid inward currents to the UV flash (131 ± 60 pA; $n = 5$) (Fig. 3*C*,*D*). However, in clear contrast to less mature cells, these uncaging currents in mature oligodendrocytes were insensitive to 30 μM CNQX (122 ± 35 pA; $n = 5$) but were entirely inhibited by the broad-spectrum glutamate transporter antagonist DL-threo-β-benzyloxyaspartic acid (TBOA) (3.5 ± 0.4 pA; $n = 3$; 100 μM) (Fig. 3*C*,*D*). Hence, during differentiation of oligodendroglial cells, there is a downregulation of AMPA/kainate receptors and an upregulation of glutamate transporters.

Although many AMPA/kainate-type receptors are still present in premyelinating oligodendrocytes, the twofold reduction in receptor number when compared with OPCs may render miniature synaptic currents undetectable in premyelinating oligodendrocytes especially because these miniature currents are already small in OPCs (Fig. 2).

To rule out this possibility, we used extracellular stimulation to synchronously activate a large number of nearby axons. Under these conditions, a robust compound response to the release of hundreds of synaptic vesicles can be recorded in a single OPC (Kukley et al., 2007). However, in contrast to the case for OPCs (Fig. 4*B*), we could not elicit any synchronous synaptic responses in 9 of 15 premyelinating oligodendrocytes. Interestingly, in 5 of 15 cells, we detected small synaptic currents, very closely resembling the quantal currents provoked by ruthenium red (Fig. 2), but the time course of their occurrence was very unusual when compared with synaptic responses in OPCs or in neurons (Fig. 4*A*,*B*). These responses occurred asynchronously and typically started to appear only 20 ms after the stimulation and continued to occur for an additional hundred milliseconds (Fig. 4*A*). The histogram in Figure 4*A*, bottom ($n = 5$), illustrates the broad distribution of the latencies which peaks at ~40–50 ms after the presynaptic action potential. The amplitude and the kinetics of these individual responses were not different from the above-mentioned amplitude of miniature synaptic currents in premyelinating oligodendrocytes, indicating that asynchronous responses are of quantal nature (amplitude, 6.2 ± 0.4 pA; rise time, 0.5 ± 0.03 ms; decay time constant, 2.1 ± 0.34 ms; $n = 5$) (Fig. 4*E*). Furthermore, these values are also not different from the amplitudes and kinetics of miniature synaptic currents in OPCs (see above) (Fig. 4*E*).

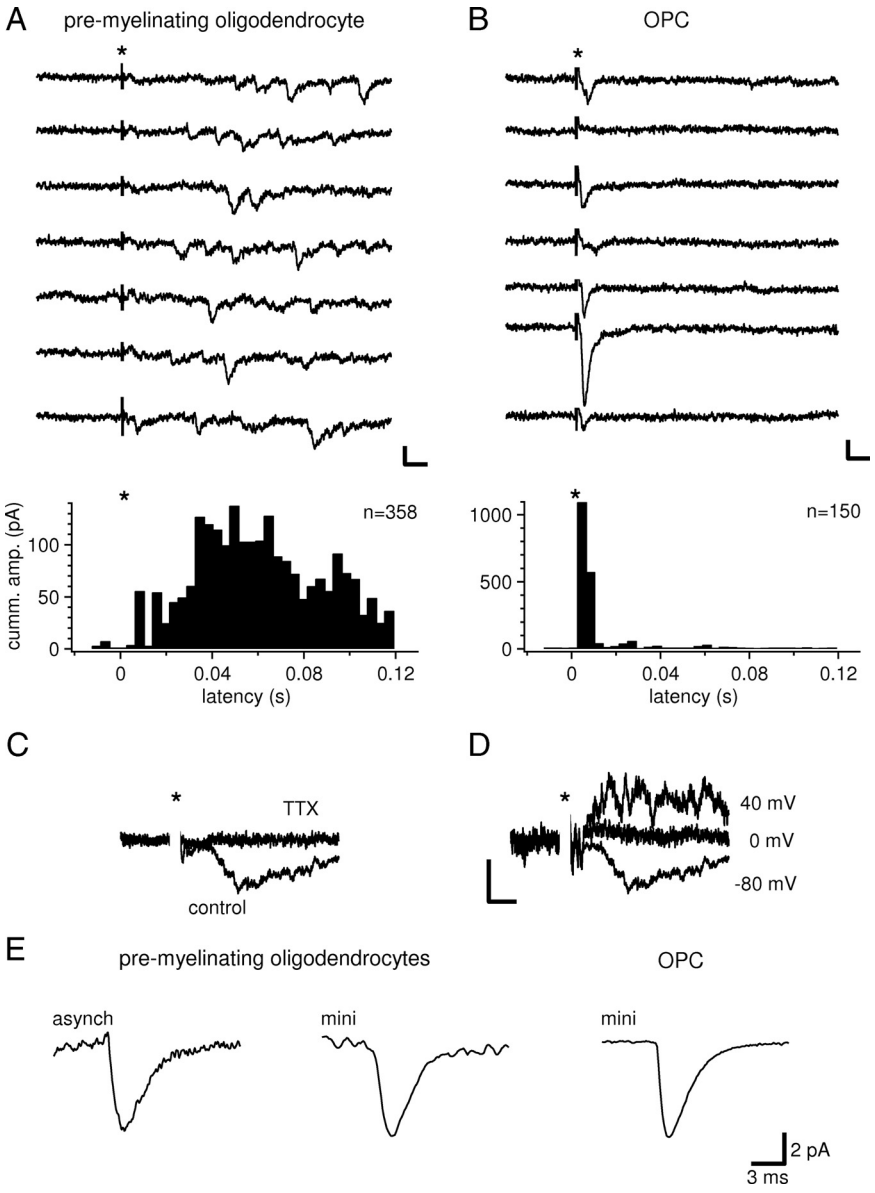

Figure 4. Transmitter release on premyelinating oligodendrocytes becomes ineffective. ***A***, Top, Extracellular electrical stimulation was used to activate axons in the neighborhood of a premyelinating oligodendrocyte (−80 mV; time point of stimulation indicated by an asterisk). The panel displays seven successive sweeps recorded in the presence of 25 μM APV and 10 μM bicuculline. We only rarely observed responses immediately after the stimulation (<5 ms; except in the bottom trace). However, asynchronous quantal responses clearly occurred with a latency of ~40 ms and continued to occur for at least a hundred milliseconds. Calibration: 10 ms, 10 pA. Stimulus artifacts have been truncated for clarity. Bottom, The histogram summarizes the latency of asynchronous synaptic currents recorded in five premyelinating oligodendrocytes (358 events). To facilitate the comparison to OPCs (in which large synchronous responses are the rule), we calculated the cumulative peak amplitude for each latency, by summing current amplitudes of all events falling into the same latency bin (bin width, 3.75 ms). ***B***, Top and bottom panels are as in ***A***, but shown for an OPC. Note that, as previously demonstrated, synaptic responses are only seen during the first few milliseconds after the stimulation ($n = 3$). Calibration: 10 ms, 10 pA. ***C***, Asynchronous synaptic currents in premyelinating oligodendrocytes are blocked by TTX. Ensemble averages of the responses recorded in the cell shown in ***A***. Calibration is as in ***D***. The asterisk indicates the time point of stimulation. The stimulus artifact has been blanked for clarity. ***D***, Asynchronous currents in premyelinating oligodendrocytes reverse around 0 mV. Ensemble averages obtained in the cell shown in ***A***. Calibration: 20 ms, 5 pA. Stimulus artifact (denoted by asterisk) has been blanked. ***E***, Asynchronous currents and miniature currents display the same kinetics and amplitudes. Left, Average of 31 individual asynchronous synaptic currents recorded in the cell shown in ***A***. Middle, Average of 9 miniature EPSCs recorded in a premyelinating oligodendrocyte. Right, Average of 400 miniature EPSCs recorded in an OPC. Calibration applies to all three traces.

As expected for AMPA/kainate receptor-mediated synaptic currents, these asynchronous synaptic currents were blocked by

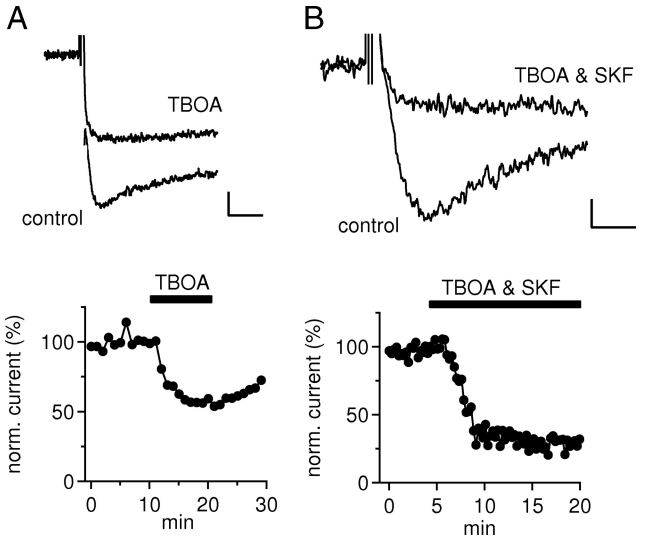

Figure 5. Myelinating oligodendrocytes clear synaptic neurotransmitter spillover. ***A***, Top, Extracellular stimulation evokes fast rising and slowly decaying inward currents in oligodendrocytes (−80 mV, holding potential). These currents are reduced by the glutamate transporter antagonist TBOA. Calibration: 10 ms, 5 pA. Bottom, Time course of the peak current amplitude of the experiment shown in the top. Note that there is only very little trial-to-trial fluctuation, indicating that the current responses are not attributable to the release of individual or a small number of vesicles. ***B***, Top, As in ***A***, but coapplication of TBOA and SKF (GABA transporter antagonist). This combined application reduces the current response to a much greater extent, indicating that oligodendrocytes take up glutamate as well as GABA. Calibration: 5 ms, 1 pA. Bottom, Time course of the peak amplitude corresponding to the experiment above.

TTX, reversed at ~0 mV (Fig. 4*C*,*D* shows the corresponding ensemble averages), and were blocked by the AMPA receptor antagonist CNQX (data not shown). For comparison, Figure 4*B* depicts the high synchrony of transmitter release onto OPCs, in which typically a single compound synaptic currents is recorded with a brief latency (<5 ms) after the stimulation (Kukley et al., 2007). In 1 of 15 premyelinating oligodendrocytes, we recorded both a prominent synchronous synaptic current immediately after the stimulation and the delayed occurring asynchronous synaptic events with a time course as shown in Figure 4*A*. We consider this cell as a transitional case between the groups of OPCs and premyelinating oligodendrocytes (data not shown).

Together, the data show that the decreased number of functional glutamate receptors alone (to ~40%) cannot account for the loss of synaptic input to premyelinating oligodendrocytes. In fact, it appears likely that changes in transmitter release properties of the presynaptic neurons are primarily responsible for this loss, whereas premyelinating oligodendrocytes are still sufficiently responsive to glutamate (for details, see Discussion).

As described above, we did not detect glutamate receptors in myelinating oligodendrocytes. Nevertheless, on uncaging of glutamate, we found pronounced currents mediated by electrogenic glutamate uptake. This opens the question of whether mature oligodendrocytes may be able to sense synaptically released glutamate by glutamate transporters. To address this question, we used the same extracellular stimulation approach used for investigating stimulated synaptic currents in premyelinating oligodendrocytes and in OPCs. To rule out unwanted side effects, we isolated neurotransmitter transporters pharmacologically by adding 10 μM CNQX, 10 μM bicuculline, and 25 μM APV to the bath solution. After only a brief delay after the extracellular stimulation (<2 ms), we recorded fast rising and slow decaying inward current that had a mean peak amplitude of 16 ± 4 pA ($n = 6$) (Fig. 5). Although these currents are of similar small size as the quantal currents recorded in OPCs and some premyelinating oligodendrocytes, their amplitudes lack the trial-to-trial fluctuation known to be associated with the statistical variability of the release of single vesicles. These currents were sensitive to the application of the glutamate transporter inhibitor TBOA (reduced to 57 ± 1%; $n = 6$; 100 μM) (Fig. 5*A*). Interestingly, the combined application of TBOA (100 μM) with the GABA transporter inhibitor *N*-(4,4-diphenyl-3-butenyl)-3-piperidine carboxylic acid [SKF 89976A (SKF)] (25 μM) (Fig. 5*B*) led to a greater inhibition of the stimulated currents (reduced to 30 ± 3%; $n = 6$), indicating that oligodendrocytes also expressed functional GABA transporters. Application of the transporter antagonists strongly slowed down the decay of the stimulated transporter currents (Fig. 5*A*,*B*, top), which is consistent with the pharmacologically reduced transmitter removal rate. Collectively, the data suggest that oligodendrocytes participate in glial uptake of neurotransmitter that has accumulated in the extracellular space after the release from many synapses.

In neurons, voltage-gated ion channels are responsible for electrical integration of synaptic input. It is known that also OPCs in brain slices express prominent amounts of voltage-gated sodium and potassium channels (Berger et al., 1991, 1992; Chvátal et al., 1995; Ge et al., 2006) (Fig. 6; supplemental Figs. 3–7, available at www.jneurosci.org as supplemental material). We therefore asked whether the above-described dramatic changes in synaptic input to oligodendroglial cells and the altered expression pattern of neurotransmitter receptors and transporters may go along with developmental alterations in the expression of voltage-gated ion channels.

Typical current patterns of the three developmental stages of oligodendroglial cells in response to a family of step depolarizations from a holding potential of −80 mV are displayed in Figure 6*A*. At first glance, it is evident that, during maturation, voltage-activated currents are strongly downregulated, whereas an ungated background conductance is strongly upregulated.

The individual subtypes of voltage-gated currents in OPCs have been identified previously, and it was shown that they express TTX-sensitive sodium currents, transient and 4-AP-sensitive potassium currents, and sustained TEA (tetraethylammonium)-sensitive potassium currents (for review, see Lin and Bergles, 2002). We estimated these three current components from the above-mentioned voltage-clamp protocol using a standard leak subtraction procedure (see Materials and Methods). In OPCs, leak subtraction regularly identified a fast rising and rapidly inactivating inward current that appeared immediately at the beginning of voltage step (Fig. 6*A*, inset). This current was TTX sensitive (data not shown) ($n = 3$) and amounted to 213 ± 43 pA ($n = 9$) (Fig. 6*A*,*B*). In some cases, this sodium current produced a net inward current, whereas in the majority of OPCs the sodium current is masked by the capacitive current after the onset of the voltage step (Fig. 6*A*) and revealed only after leak subtraction. The transient and the sustained potassium currents in OPCs amounted to 1270 ± 140 and 490 ± 49 pA, respectively ($n = 10$) (Fig. 6*A*,*B*).

The current pattern of premyelinating oligodendrocytes is also dominated by outward currents of similar magnitude and apparently closely resembles that of OPCs (Fig. 6*A*,*B*). However, in premyelinating oligodendrocytes, the leak subtraction procedure failed to reveal any voltage-activated sodium channels (Fig. 6*A*, inset, on the top right). Only two of nine cells showed a small residual inward current such that the average sodium current in premyelinating oligodendrocytes was reduced by a factor of 10 when compared with OPCs (26 ± 20 pA; $n = 9$) (Fig. 6*B*).

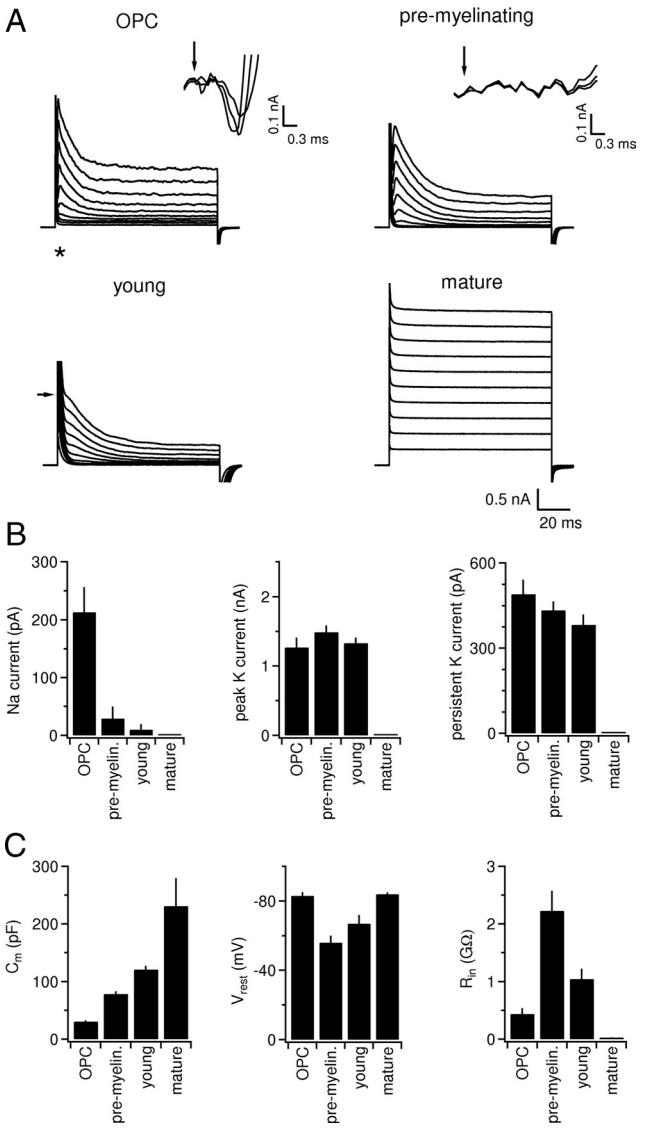

Figure 6. Loss of synaptic input is accompanied by a specific loss of voltage-gated sodium currents. ***A***, Whole-cell current pattern of four different developmental stages of oligodendroglial cells with potassium as the main internal cation. From a holding potential of −80 mV, cells were depolarized in steps of 10 mV up to +20 mV. The calibration is the same for the four current families and is given in the right bottom corner. Only in OPCs did we detect a transient fast inward current soon after the beginning of the voltage step, which closely resembled voltage-activated sodium currents. The time point of this current is indicated by the asterisk in the top left. Note that, in many cases, the sodium current is masked by the transient capacitive currents such that the sodium current is revealed only after leak subtraction. The insets in the top row show leak subtracted current traces at an expanded time calibration for the voltage steps from the holding potential of −80 mV to 0, +10, and +20 mV (the arrows indicate the beginning of voltage step). The right inset displays that, even after leak subtraction, no inward current is apparent in premyelinating oligodendrocytes. The horizontal arrow placed next to the current families of a young oligodendrocyte indicates the peak of the voltage-activated potassium currents, which partially superimposes with the capacitive current because of the increase in cell capacitance at this developmental stage. Mature oligodendrocytes show a pure ohmic current response. The capacitive current transients have been truncated for clarity throughout this figure. ***B***, Summary bar graphs of the peak amplitudes of the three current components analyzed at each of the four developmental stages. Voltage-activated sodium currents are lost as soon as OPCs differentiate, whereas voltage-activated potassium currents remain present in young oligodendrocytes and are only lost once a cell has fully matured and built up many myelin sheaths. ***C***, Summary of the passive membrane properties quantified in each of the four developmental stages. Note the significant increase in input resistance in premyelinating oligodendrocytes and the dramatic drop of input resistance on the transition to mature oligodendrocytes. Error bars indicate SEM.

To better illustrate the gradual change of ion channel expression and membrane properties over development, we divided the group of myelinating oligodendrocytes in young and mature myelinating oligodendrocytes for the purpose of this figure. The group of young oligodendrocytes comprised cells that showed one to six myelin sheaths (compare for Fig. 1*D*), whereas mature oligodendrocytes were defined as cells displaying more than six myelin sheaths. Young oligodendrocytes (Fig. 6*A*) still show similar levels of outward currents, but sodium currents are further reduced compared with OPCs (in only 1 of 10 cells fast inward currents were detected) (Fig. 6*B*).

In agreement with previous reports, the most substantial changes in current pattern were observed in mature oligodendrocytes (Fig. 6), which did not express any detectable levels of voltage-gated ion channels but instead expressed a profound ungated background conductance as also reported in astrocytes (Chvátal et al., 1995).

During development, the passive electrical properties of oligodendroglial are strongly modified. The membrane capacitance (C_m), which is a measure of the cell surface area, continuously increases from a value of ~30 pF in OPCs to ~230 pF in mature oligodendrocytes (Fig. 6*C*). This is expected for the morphological transformation of OPCs into oligodendrocytes because the complexity of the tree of processes steadily increases. Because the major morphological difference between young and mature myelinating oligodendrocytes is the number of myelin sheaths, it is likely that these additional sheaths are responsible for the observed increase in membrane.

The relatively high input resistance of OPCs (R_m, 436 ± 100 MΩ; $n = 10$) strongly increases further to a value of 2230 ± 350 MΩ ($n = 9$) when the cells differentiate into premyelinating oligodendrocytes, and then declines on additional differentiation. Eventually, R_m drops in mature oligodendrocytes and reaches very low values, which are only known from astrocytes (23 ± 6 MΩ; $n = 13$) (Fig. 6*C*). The developmental changes in R_m are mirrored by concomitant changes in the resting membrane potential (V_{rest}), suggesting that the changes in R_m are attributable to upregulation and downregulation of ungated potassium channels (Fig. 6*C*).

Discussion

Synaptic input to OPCs has been described in various regions of the CNS, but the fate of these synapses when OPCs differentiate was unknown. The main findings of the present study are that synaptic input is restricted to OPCs and is lost on their additional differentiation into immature oligodendrocytes. Our data suggest that the loss of synaptic currents in premyelinating oligodendrocytes is attributable to the disassembly of the release machinery in the presynaptic axon. This indicates that neurons are able to discern different developmental stages of postsynaptic oligodendroglial cells and to differentially regulate transmitter release onto different subtypes of glial cells and onto other neurons (Fig. 7). Furthermore, the loss of synaptic input is accompanied by a dramatic developmental downregulation of voltage-gated sodium channels in oligodendroglial cells hinting at their role in electrical integration of synaptic input. Finally, we show that mature oligodendrocytes participate in homeostatic functions such as uptake of neurotransmitter.

Loss of synaptic input to premyelinating oligodendrocytes is initiated presynaptically

Uncaging glutamate showed that premyelinating oligodendrocytes express only one-half the number of functional AMPA/

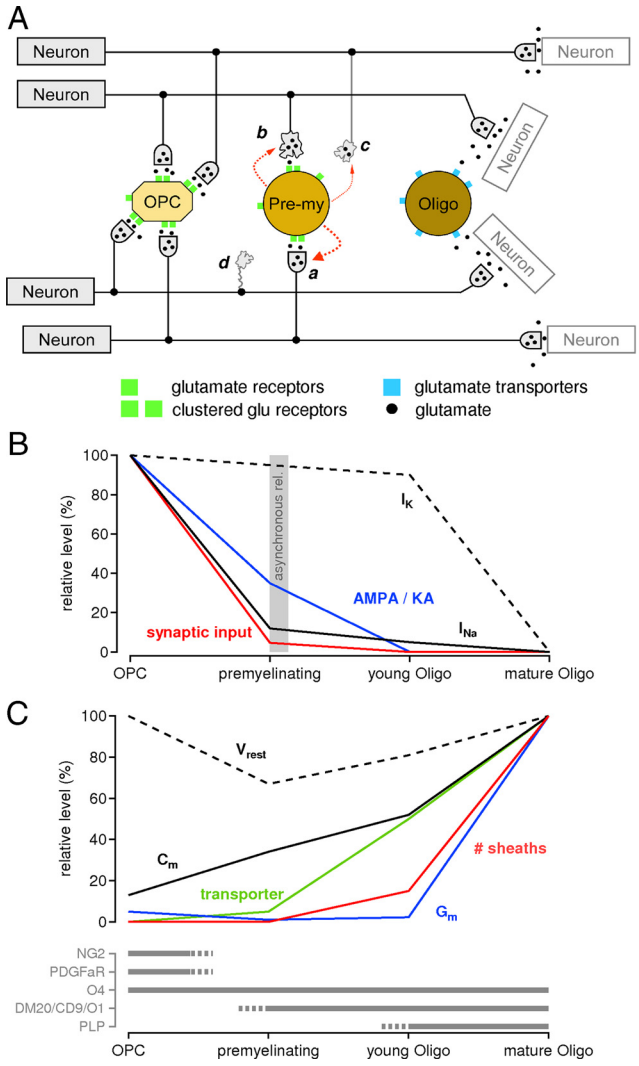

Figure 7. Diagram and synopsis illustrating how synaptic connectivity and function of oligodendroglial cells changes over development. ***A***, In this example, created to illustrate our interpretation of the experimental results, the neural network consists of four presynaptic neurons on the left that project onto four neurons on the right. The black and gray lines indicate axons and axonal collaterals. In the middle of the figure, three developmental stages of oligodendroglial cells are depicted (OPC; premyelinating oligodendrocyte, Pre-my; mature oligodendrocyte, Oligo). OPCs receive synapses from neighboring neurons that release transmitter onto clustered glutamate receptors. Once an OPC has differentiated into a premyelinating oligodendrocyte, it transmits a retrograde signal (red dashed arrows) to the presynaptic neurons, which triggers the disassembly of the presynaptic terminal. ***a*** represents a synaptic terminal that is still fully functional, whereas ***b*** indicates a terminal that has partially been disassembled and that ineffectively releases vesicles in an asynchronous fashion. Note that glutamate receptors (in this context: AMPA/kainate receptors) remain clustered at this stage (asynchronous events show the same quantal amplitude as miniature EPSCs in OPCs). In ***c*** and ***d***, the process of disassembly has proceeded such that no transmitter can be released from these terminals. At this stage, glutamate receptors are removed from the surface (overall receptor number is halved in premyelinating oligodendrocytes compared with OPCs). On additional maturation, myelinating oligodendrocytes almost entirely downregulate glutamate receptors and started to express glutamate transporters. Glutamate transporters are activated by neurotransmitter that has been released at the neighboring synapses. Note that an individual axonal branch contacts neurons and different stages of oligodendroglial cells, which illustrates the necessity for a local regulation of the transmitter release machinery and of the presynaptic terminals. ***B***, Properties that are downregulated during development. The first changes on differentiation of OPCs are the loss of synaptic input and the downregulation of sodium channels. Note that the downregulation of voltage-activated potassium currents lags significantly behind the downregulation of voltage-gated sodium currents. The gray area indicates the transient period during which asynchronous transmitter release can be observed in a small fraction of premyelinating oligodendrocytes. ***C***, Top, Properties that are upregulated during development. It is probably cell growth and the acquisition of sheaths during development that cause C_m to increase and R_{in} to decrease ($R_{in} = 1/G_m$). Bottom, The bars indicate the time points during which the corresponding markers are expressed.

kainate receptors as compared to OPCs. However, the reduced number of glutamate receptors cannot explain the almost complete lack of synchronous synaptic currents in response to electrical stimulation: on stimulation, many hundreds of axons are activated and typically produce pronounced synaptic currents (hundreds of picoamperes), which would still by far exceed the detection threshold in our recordings (~3–5 pA) even when reduced by one-half. In fact, the quantal current amplitude in the very few premyelinating oligodendrocytes that show synaptic responses was quite comparable with that in NG2 cells (compare Figs. 2, 4), suggesting that glutamate receptors remain clustered beneath residual functional release sites (Fig. 7) and that the disappearance of synaptic currents is rather attributable to presynaptic changes. This view is further supported by our observation that the action potential-triggered presynaptic release rate, in the few premyelinating oligodendrocytes with synaptic input, showed extremely slow kinetics (Fig. 4) such that most of the released vesicles did not coincide and appear asynchronously.

The comparable quantal amplitude in OPCs and premyelinating cells can be viewed as evidence for comparable synaptic glutamate concentrations, for comparable glutamate affinity and comparable conductance of synaptic receptors. If we assume that ruthenium red is equally effective in both types of cells, then the 20-fold decrease in the frequency of miniature synaptic currents recorded in premyelinating oligodendrocytes is opposed to a 2-fold reduction in the total number of glutamate receptors, as assessed by uncaging experiments. This means that, in the small proportion of premyelinating oligodendrocytes that display a residual synaptic input, the percentage of receptors being activated by synaptic glutamate is 10-fold smaller when compared to OPCs. Our interpretation of this situation is that neurons first stop releasing transmitter onto differentiating oligodendroglial cells, whereas the removal of unused/extrasynaptic receptors from the cell surface follows at a slower rate (Fig. 7).

It may be argued that the increased complexity of the tree of processes of premyelinating oligodendrocytes may render synaptic currents undetectable by electrotonic filtering. However, a strong electrotonic filtering is not compatible with our experimental observations: in case of strong filtering, the abovementioned electrical stimulation of hundreds of axons should have produced a large and slow compound synaptic current, but we observed individual small and fast asynchronous synaptic currents (Fig. 4). Furthermore, these asynchronous synaptic currents were also not different in amplitude, rise time, or decay time constant from quantal currents recorded in OPCs. The absence of obvious electrotonic filtering is most likely be explained by the fact that the increased complexity of processes in premyelinating cells is mostly attributable to more processes (rather than to longer processes) and that processes in premyelinating cells display a greater diameter (supplemental Fig. 2, available at www.jneurosci.org as supplemental material).

Disassembly of release apparatus may underlie loss of synaptic input

We propose that the asynchronous synaptic currents encountered in a minority of premyelinating oligodendrocytes represent the residual and transient function of release machinery that is in the process of being altered and hint at the mechanism by which neuron–glia synapses may be disassembled. Previously, we showed that, in neuron–OPC synapses, as it is known from neuron–neuronal synapses, the rate of release sharply increases very soon after the presynaptic action potential (<1 ms), peaks shortly thereafter, and declines back to baseline levels within 3–5 ms

(Kukley et al., 2007). Such a highly synchronized transmitter release rate requires the full complement of presynaptic fusion proteins and a short-lived calcium signal at the release sensor during an action potential (Schneggenburger and Neher, 2000; Sun et al., 2007). Interestingly, transmitter release at neuronal synapses can be desynchronized if these conditions are not met: experimentally slowing and reducing the calcium signal seen by the sensor or removing important components of the presynaptic release machinery leads to the appearance of asynchronous synaptic currents and dramatically reduces synchronous transmitter release (Schneggenburger and Neher, 2000; Xu-Friedman and Regehr, 2000; Sun et al., 2007). Therefore, one mechanism of the desynchronization of transmitter release might be that the calcium microdomain signaling between channels and the release sensor is disrupted by removing the channels from the immediate vicinity of the release machinery. Transmitter release rate may then follow the slow and weak calcium signals originating from remote calcium channels only. A second mechanism may be that the disassembly of synapses contacting a premyelinating oligodendrocyte starts with the removal of a calcium sensor protein that is essential for synchronous transmitter release, in analogy to the findings in synaptotagmin-2 knock-out mice (Sun et al., 2007). However, although we view these two mechanisms as possible first steps in the process of a complete synapse disassembly, it should be noted that it is compatible with our experimental results that calcium channels or presynaptic proteins are just rearranged without major changes in the structure of the synapses (i.e., without a complete disassembly of the synapse).

An alternate explanation of the occurrence of asynchronous synaptic currents may be that they are attributable to network activity (i.e., attributable to asynchronously firing neurons in the hippocampal network). Although this is principally possible, we believe it is quite unlikely because (1) a single extracellular stimulation of Schaffer collaterals does not induce network activity, especially when NMDA receptors are blocked (APV was present); (2) such asynchronous synaptic currents were never observed in OPCs, although they are coexisting in the same subfields and are more tightly integrated in the hippocampal synaptic circuitry; and (3) the absence of an early, synchronous synaptic current immediately after the stimulation in premyelinating oligodendrocytes is difficult to reconcile with a strong activation of the surrounding neuronal network.

Regulation of synapses depends on the developmental state of the postsynaptic glial cell

We and others did not observe asynchronous transmitter release onto OPCs (Bergles et al., 2000; Kukley et al., 2007; Ziskin et al., 2007). This implies that neurons recognize the developmental stage of the postsynaptic glial cell and are able to selectively disassemble the release machinery at contact sites to differentiating oligodendroglial cells (Fig. 7). Furthermore, it appears likely that the process of synaptogenesis is specific with respect to the developmental stage of the glial cells: On the one hand, neurons in the postnatal brain continuously establish new synapses with newborn OPCs (Kukley et al., 2008; Ge et al., 2009), whereas, on the other hand, neurons do not establish new synapses onto coexisting premyelinating oligodendrocytes, although the latter are probably sufficiently responsive to synaptically released glutamate. Therefore, the present study supports the view that synaptic contacts on OPCs represent a specific cell–cell interaction rather than promiscuous synaptogenesis onto glutamate receptor-containing membranes in a synapse-permissive environment such as the hippocampus.

Does cessation of transmitter release trigger the differentiation of OPCs?

The finding that oligodendroglial cells lose synaptic input as soon as they differentiate raises the question of whether the removal of synaptic input may act to trigger their differentiation. It is reasonable to assume that the transformation of an OPC into a premyelinating oligodendrocyte takes at least 1 d because there are substantial morphological differences. For this reason, a given cell would be expected to keep the identity of an OPC for at least 1 d after the process of differentiation has been triggered by the removal of synaptic input. This implies that we should have observed a fraction of OPCs that lacks synaptic input and possibly another fraction that receives asynchronous synaptic input. Furthermore, synaptic currents should then be entirely absent in premyelinating oligodendrocytes. On the contrary, all OPCs display synchronous synaptic currents (Bergles et al., 2000; Lin and Bergles, 2004; Kukley et al., 2007, 2008; Ziskin et al., 2007) and there is a fraction of premyelinating oligodendrocytes exhibiting asynchronous synaptic currents. Therefore, our data do not suggest that dismantling the release machinery triggers the differentiation of OPCs but rather indicate that premyelinating oligodendrocytes may use a retrograde signal to disclose their new developmental stage to the presynaptic neuron.

Although, as outlined above, the removal of synaptic input itself is unlikely to modulate the time point of differentiation, it is important to note that it is still possible that a certain pattern of synaptic transmitter release onto OPCs does play a part in triggering differentiation. Furthermore, it is also conceivable that synaptic input to an OPC triggers long-term changes that come into action only once the cell has proceeded to later developmental stages.

How do mature oligodendrocytes *in vivo* respond to glutamate?

Numerous reports have shown that cultured oligodendrocytes express AMPA/kainate receptors (for review, see Kettenmann and Steinhaeuser, 2005). This is in striking contrast to the present study in which we were not able to detect AMPA/kainate receptors in oligodendrocytes in native tissue. Instead of receptor currents, our uncaging experiments revealed a substantial glutamate transporter current in mature oligodendrocytes (Fig. 3). This is in good agreement with a previous study using a similar photolytic technique on oligodendrocytes (Regan et al., 2007) and with previous reports investigating the expression of glutamate transporter proteins and glutamate uptake rates in oligodendrocytes (Arranz et al., 2008; DeSilva et al., 2009). Interestingly, our experiments with synaptic stimulation (Fig. 5) also showed that these oligodendroglial glutamate transporters contribute to the removal of synaptically released transmitter and that they do so not only for glutamate but also for GABA. However, it is important to point out that, although oligodendrocytes sense neurotransmitter release via electrogenic transporter currents, they are not able to discriminate release events from single synapses (i.e., the release of individual vesicles). First, under conditions that provoked spontaneous release of individual vesicles (Fig. 2), we never registered any spontaneous currents in mature oligodendrocytes. Second, stimulated transporter currents lacked failures and the trial-to-trial fluctuation typically associated with the probabilistic nature of the release of individual vesicles. Therefore, the fundamental difference between neuron-to-OPC and neuron-to-oligodendrocyte signaling is that oligodendrocytes only detect transmitter that pools in the extracellular space, presumably released from many hundreds of synapses.

References

Arranz AM, Hussein A, Alix JJ, Pérez-Cerdá F, Allcock N, Matute C, Fern R (2008) Functional glutamate transport in rodent optic nerve axons and glia. Glia 56:1353–1367.

Berger T, Schnitzer J, Kettenmann H (1991) Developmental changes in the membrane current pattern, K^+ buffer capacity, and morphology of glial cells in the corpus callosum slice. J Neurosci 11:3008–3024.

Berger T, Schnitzer J, Orkand PM, Kettenmann H (1992) Sodium and calcium currents in glial cells of the mouse corpus callosum slice. Eur J Neurosci 4:1271–1284.

Bergles DE, Roberts JD, Somogyi P, Jahr CE (2000) Glutamatergic synapses on oligodendrocyte precursor cells in the hippocampus. Nature 405:187–191.

Chvátal A, Pastor A, Mauch M, Syková E, Kettenmann H (1995) Distinct populations of identified glial cells in the developing rat spinal cord slice: ion channel properties and cell morphology. Eur J Neurosci 7:129–142.

DeSilva TM, Kabakov AY, Goldhoff PE, Volpe JJ, Rosenberg PA (2009) Regulation of glutamate transport in developing rat oligodendrocytes. J Neurosci 29:7898–7908.

Fuss B, Mallon B, Phan T, Ohlemeyer C, Kirchhoff F, Nishiyama A, Macklin WB (2000) Purification and analysis of in vivo-differentiated oligodendrocytes expressing the green fluorescent protein. Dev Biol 218:259–274.

Gallo V, Mangin JM, Kukley M, Dietrich D (2008) Synapses on NG2-expressing progenitors in the brain: multiple functions? J Physiol 586:3767–3781.

Ge WP, Yang XJ, Zhang Z, Wang HK, Shen W, Deng QD, Duan S (2006) Long-term potentiation of neuron-glia synapses mediated by Ca^{2+}-permeable AMPA receptors. Science 312:1533–1537.

Ge WP, Zhou W, Luo Q, Jan LY, Jan YN (2009) Dividing glial cells maintain differentiated properties including complex morphology and functional synapses. Proc Natl Acad Sci U S A 106:328–333.

Káradóttir R, Hamilton NB, Bakiri Y, Attwell D (2008) Spiking and nonspiking classes of oligodendrocyte precursor glia in CNS white matter. Nat Neurosci 11:450–456.

Kettenmann H, Steinhaeuser C (2005) Receptors for neurotransmitters and hormones. In: Neuroglia (Kettenmann H, Ransom BR, eds), pp 131–145. New York: Oxford UP.

Kukley M, Dietrich D (2009) Kainate receptors and signal integration by NG2 glial cells. Neuron Glia Biol 22:1–8.

Kukley M, Capetillo-Zarate E, Dietrich D (2007) Vesicular glutamate release from axons in white matter. Nat Neurosci 10:311–320.

Kukley M, Kiladze M, Tognatta R, Hans M, Swandulla D, Schramm J, Dietrich D (2008) Glial cells are born with synapses. FASEB J 22:2957–2969.

Lin SC, Bergles DE (2002) Physiological characteristics of NG2-expressing glial cells. J Neurocytol 31:537–549.

Lin SC, Bergles DE (2004) Synaptic signaling between GABAergic interneurons and oligodendrocyte precursor cells in the hippocampus. Nat Neurosci 7:24–32.

Mallon BS, Shick HE, Kidd GJ, Macklin WB (2002) Proteolipid promoter activity distinguishes two populations of NG2-positive cells throughout neonatal cortical development. J Neurosci 22:876–885.

Mangin JM, Kunze A, Chittajallu R, Gallo V (2008) Satellite NG2 progenitor cells share common glutamatergic inputs with associated interneurons in the mouse dentate gyrus. J Neurosci 28:7610–7623.

Müller J, Reyes-Haro D, Pivneva T, Nolte C, Schaette R, Lübke J, Kettenmann H (2009) The principal neurons of the medial nucleus of the trapezoid body and $NG2^+$ glial cells receive coordinated excitatory synaptic input. J Gen Physiol 134:115–127.

Nishiyama A, Komitova M, Suzuki R, Zhu X (2009) Polydendrocytes (NG2 cells): multifunctional cells with lineage plasticity. Nat Rev Neurosci 10:9–22.

Novak A, Guo C, Yang W, Nagy A, Lobe CG (2000) Z/EG, a double reporter mouse line that expresses enhanced green fluorescent protein on Cre-mediated excision. Genesis 28:147–155.

Regan MR, Huang YH, Kim YS, Dykes-Hoberg MI, Jin L, Watkins AM, Bergles DE, Rothstein JD (2007) Variations in promoter activity reveal a differential expression and physiology of glutamate transporters by glia in the developing and mature CNS. J Neurosci 27:6607–6619.

Schneggenburger R, Neher E (2000) Intracellular calcium dependence of transmitter release rates at a fast central synapse. Nature 406:889–893.

Shepherd GM, Harris KM (1998) Three-dimensional structure and composition of CA3→CA1 axons in rat hippocampal slices: implications for presynaptic connectivity and compartmentalization. J Neurosci 18:8300–8310.

Sommer I, Schachner M (1981) Monoclonal antibodies (O1 to O4) to oligodendrocyte cell surfaces: an immunocytological study in the central nervous system. Dev Biol 83:311–327.

Sun J, Pang ZP, Qin D, Fahim AT, Adachi R, Südhof TC (2007) A dual-Ca^{2+}-sensor model for neurotransmitter release in a central synapse. Nature 450:676–682.

Tong XP, Li XY, Zhou B, Shen W, Zhang ZJ, Xu TL, Duan S (2009) Ca^{2+} signaling evoked by activation of Na^+ channels and Na^+/Ca^{2+} exchangers is required for GABA-induced NG2 cell migration. J Cell Biol 186:113–128.

Trapp BD, Nishiyama A, Cheng D, Macklin W (1997) Differentiation and death of premyelinating oligodendrocytes in developing rodent brain. J Cell Biol 137:459–468.

Xu-Friedman MA, Regehr WG (2000) Probing fundamental aspects of synaptic transmission with strontium. J Neurosci 20:4414–4422.

Yuan X, Eisen AM, McBain CJ, Gallo V (1998) A role for glutamate and its receptors in the regulation of oligodendrocyte development in cerebellar tissue slices. Development 125:2901–2914.

Zhu X, Bergles DE, Nishiyama A (2008a) NG2 cells generate both oligodendrocytes and gray matter astrocytes. Development 135:145–157.

Zhu X, Hill RA, Nishiyama A (2008b) NG2 cells generate oligodendrocytes and gray matter astrocytes in the spinal cord. Neuron Glia Biol 4:19–26.

Ziskin JL, Nishiyama A, Rubio M, Fukaya M, Bergles DE (2007) Vesicular release of glutamate from unmyelinated axons in white matter. Nat Neurosci 10:321–330.